J. Physiol. (1987), **386**, *pp.* 219–246
With 9 text-figures
Printed in Great Britain

THE DYNAMICS OF THE CAT RETINAL X CELL CENTRE

BY JONATHAN D. VICTOR

From the Department of Neurology, Cornell University Medical College, 1300 York Avenue, New York City, New York 10021, U.S.A. and Laboratory of Biophysics, The Rockefeller University, 1230 York Avenue, New York City, New York 10021, U.S.A.

(*Received 24 April 1986*)

SUMMARY

1. The dynamics of the centre mechanism of individual cat X retinal ganglion cells is investigated. The visual stimuli consist of temporal contrast modulation of stationary patterns. In order to study the response of the centre mechanism, patterns were either sine gratings of high spatial frequency or small circular spots positioned over the receptive-field centre.

2. Responses to contrast reversal are approximately linear. However, as the modulation depth of the stimulus increases, responses become more transient. Ganglion cell responses show this phenomenon at moderate contrasts (e.g. 0·1), which do not elicit discharges that approach the maximum firing rate of the ganglion cell.

3. A sequence of dynamical models are constructed from responses elicited by sum-of-sinusoids modulation of the spatial pattern. The first model is strictly linear. It consists of a series of low-pass filters and a single high-pass filter. The linear model predicts the approximate shape of the step response, but does not account for the change in shape of the response as a function of modulation depth.

4. The second model, a quasi-linear model, allows the 'linear' dynamics to vary slowly with a neural measure of contrast. The main effect of high contrast is a shorter time constant in the high-pass filter. This model accounts qualitatively for the increased transience of the response, but fails to predict the magnitude of the effect at higher modulation depths.

5. In the third model, the transfer characteristics of the centre response adjust rapidly as contrast changes. This intrinsically non-linear model provides excellent agreement with observed response to steps and more complex modulation patterns.

6. The non-linearity necessitated by a voltage-to-spikes transduction is analysed quantitatively. In most ganglion cells, a simple truncation at 0 impulses/s (and no saturation) explains the changes in apparent gain and mean firing rate that occur as modulation depth is increased. A non-linear voltage-to-spike transduction *per se* cannot account for the observed effect of contrast on dynamics.

7. The parameters of the dynamical model are measured for a population of twenty-seven X ganglion cells (nineteen on-centre and eight off-centre). The low-pass stage and the strength of the high-pass stage are relatively uniform across the population. The over-all gain and the dynamics of the high-pass stage vary substantially across the population, but show no consistent dependence on the on–off

distinction or on retinal location. Some implications of this variability for retinal function are discussed.

INTRODUCTION

The output neurones of the retinal network are objects of intense scrutiny. A detailed knowledge of retinal information processing is a prerequisite for the study of more central stages of visual processing. In addition, the receptive-field structure of the retinal ganglion cell serves as a model for neural integration in general. In the cat, the retinal ganglion cells that form the start of the geniculo-calcarine pathway fall into two qualitatively distinct categories: X and Y. Although this distinction (Enroth-Cugell & Robson, 1966) was originally made on the basis of a qualitative description of spatial summation (X: linear, Y: non-linear), it is clear that X and Y cells also have different dynamics (Cleland, Dubin & Levick, 1971), different spatial scales (Enroth-Cugell & Robson, 1966; Cleland, Levick & Sanderson, 1973), different conduction velocities (Stone & Fukuda, 1974) and different morphologies (Boycott & Wässle, 1974).

The separation of visual information into two distinct streams has major functional importance (Lennie, 1980). Yet, the relationship of the linear–non-linear distinction to the sustained–transient distinction is an open question. In principle, receptive-field elements of X and Y cells might have similar intrinsic dynamics, and the non-linearities of spatial summation in the Y cell could result in more transient response dynamics. Alternatively, the intrinsic dynamics of X and Y cell receptive-field mechanisms may be different, and thus lead to the difference in response dynamics. A related question is the functional role of the Y cell non-linearity. To address these issues, a detailed knowledge of both X and Y receptive-field dynamics is needed.

Such detailed knowledge is best represented as a model of response dynamics which accurately predicts responses of ganglion cells to a wide range of stimuli. For the X cell, one might hope that a linear model would fulfill this need. Unfortunately, a linear model does not explain all of the salient features of the X cell response (Shapley & Victor, 1978).

This paper examines the dynamics of the X cell centre, and focuses on linear models and the deviations from linearity. *A priori*, several non-linearities – including light adaptation, the contrast gain control, and the non-linearity which is a consequence of the requirement that a firing rate is non-negative – can influence response dynamics. Simple qualitative experiments permit one to estimate the relative importance of these non-linearities. Light adaptation does not appear to be important in the 10–25 % contrast range. The other two phenomena, the contrast gain control and the truncation of the impulse rate at 0 impulses/s, have effects on the response dynamics in this contrast range.

A second level of analysis incorporates these notions into a predictively accurate model of the centre's dynamics. This model is based on a quantitative comparison of response to complex, broad-band modulation patterns (the sum-of-sinusoids) and step responses. Although this model is intrinsically non-linear, it predicts nearly sinusoidal responses to sinusoidal inputs. The non-linearity is essential for accurate prediction of the dynamics of the responses to moderate steps of contrast and other patterns of contrast modulation.

METHODS

Physiological methods

Recordings of single retinal ganglion cell activity were made in fifteen adult male and female cats. The physiological preparation was similar to that used in previous studies (Hochstein & Shapley, 1976*a*). Anaesthesia was induced with ketamine (10 mg/kg, I.M.) and maintained during surgery with sodium thiamylal administered I.V. as needed. Lidocaine, 1 %, was infiltrated at all of the surgical sites. Pupils were dilated and nictitating membranes were retracted with phenylephrine, 10 %, and atropine sulphate, 1 %. Cannulae were placed in both femoral veins for drug administration and in one femoral artery for blood pressure monitoring. A tracheal cannula was inserted for mechanical ventilation and the cervical sympathetics were divided to minimize eye movement (Rodieck, Pettigrew, Bishop & Nikara, 1967). Penicillin in depot form (150000 u I.M.) and dexamethasone (2 mg/kg, I.V.) were administered prophylactically. During physiological recording, anaesthesia was maintained with urethane (0·2 g/kg, I.V. loading, 0·1 g/(kg.24 h), I.V. maintenance) and paralysis was induced with gallamine triethiodide (5 mg/kg h), I.V.). During paralysis, depth of anaesthesia was monitored by blood pressure, heart rate, electroencephalogram (e.e.g.) and salivation. Blood pressure was maintained above 90 mmHg with fluids if needed; end-expiratory carbon dioxide was maintained in the range 3·0 to 3·5 % as monitored on a Beckman LB2 Medical Gas Analyzer; and temperature was maintained at 38–39 °C by a heating pad controlled by a thermistor inserted behind the scapula. Glucose and oxygen were administered periodically. The corneas, protected with contact lenses with a 3 mm diameter artificial pupil, were lavaged periodically with saline.

Ringer solution-filled pipette micro-electrodes (typical resistance, 10–30 MΩ) were used to record single-unit activity of retinal ganglion cells, either as axon spikes in the optic tract, or as unitary S-potential activity in the dorsal lateral geniculate nucleus (Kaplan & Shapley, 1984). In either case, the electrode was advanced vertically through a burr hole at or near Horsley–Clarke coordinates (9 A, 9 L) until single-unit activity could be reliably discriminated above the background neural activity by its height. The receptive field of the unit was mapped on a tangent screen, and the unit was classified as X or Y by its response to a high-spatial-frequency grating (Hochstein & Shapley, 1976*a*). Refraction was corrected by trial lenses chosen to optimize the unit's response to fine patterns. The spatial frequency resolution of the unit was determined by listening to the response to square-wave contrast reversal at 2 Hz or drift at 2 bars/s of high-spatial-frequency gratings at a contrast of 0·5. Thresholds determined in this manner correlate well with thresholds determined from more rigorous analysis of the signal-to-noise ratio of the square-wave response (Shapley & Victor, 1986). For quantitative study, a discriminator circuit was set to send pulses to the computer at each occurrence of an action potential of the isolated unit. The number of pulses during each frame of the display (3·699 ms) was recorded on-line by a PDP 11/23 computer for subsequent analysis.

Stimulus description

Visual stimuli were realized on a Tektronix 608 display oscilloscope with a fast white (P4) phosphor. The *X* (horizontal), *Y* (vertical), and *Z* (intensity) voltages were generated by specialized electronics (Milkman, Schick, Rossetto, Ratliff, Shapley & Victor, 1980) interfaced to the PDP 11/23 computer which recorded impulse arrivals. This apparatus provided for control of a 256 × 256 pixel raster display at a frame rate of 270·3 Hz. The raster has a mean luminance of 100 cd/m^2, with the *Z* input of the oscilloscope modified so that luminance is linear as a function of voltage for variations around the mean of up to 50 %.

All visual stimuli consisted of a stationary pattern whose contrast varied in time. In most of the experiments, the pattern was a spatial sine grating whose spatial frequency was chosen to be half of the highest spatial frequency resolved by the unit. For units that demonstrated orientational bias (Levick & Thibos, 1982), the grating was oriented for optimum resolution. For units without appreciable orientational bias, the grating was vertical. In some of the experiments, the stimulus consisted of a circular spot positioned over the receptive-field centre. The diameter of the spot was equal to half the period of the grating of highest resolvable spatial frequency.

Data collection was segmented into a sequence of 35 s episodes. The first 5 s of the response to each stimulus pattern were discarded; the remaining 30·3 s (8192 frames) comprise the data saved

for later study. Episodes were of two types: 'analysis' and 'synthesis'. The analysis episodes provided data from which model parameters were determined; the synthesis episodes provided measurements of responses to unrelated temporal patterns and provided for testing of the model.

In all episodes, the average luminance over both space and time was a constant value $L_0 = 100$ cd/m^2. The fractional deviation from this mean luminance (the signed Weber fraction) was equal to a product of a fixed spatial function (a grating or a spot, denoted $q(X, Y)$) and a temporal modulation signal $s(t)$. Thus, the luminance $L(X, Y, t)$ of the stimulus at a point (X, Y) and time t is given by

$$L(X, Y, t) = L_0 [1 + s(t) . q(X, Y)]. \tag{1}$$

The temporal modulation signal $s(t)$ is either an analysis signal $s_{\text{anal}}(t)$ or a synthesis signal $s_{\text{syn}}(t)$, as described below. The maximum excursion of the spatial function $q(X, Y)$ was equal to 1, and was always over the receptive-field centre (by convention at $(X, Y) = (0, 0)$. For example, a grating of spatial frequency k was specified by the spatial function $q(X, Y) = \cos(2\pi kX)$.

The models which will be developed below will have the (signed) Weber fraction as their input (see Discussion). For all stimuli used in these studies, either the (spatial) average of the spatial function $q(X, Y)$ was zero, or the (temporal) average of the modulation signal $s(t)$ was zero, or both. Thus, the signed Weber fraction at the receptive-field centre is always equal to the temporal modulation signal $s(t)$.

The temporal modulation signal for the analysis episodes, $s_{\text{anal}}(t)$, was a sum of sinusoids at eight nearly incommensurate frequencies f_j:

$$s_{\text{anal}}(t) = m_{\text{anal}} \sum_{j=1}^{8} \cos(2\pi f_j t + \phi_j). \tag{2}$$

In this equation, m_{anal} is the modulation depth produced by each sinusoidal component. The eight frequencies f_j are approximately equally spaced logarithmically: 0·231, 0·495, 1·023, 2·079, 4·191, 8·415, 16·863 and 33·758 Hz. These frequencies are exact integer multiples (7, 15, 31, 63, 127, 255, 511 and 1023) of the common fundamental frequency 0·032999 Hz. The phases ϕ_j are all $+\pi/2$ or $-\pi/2$. For each presentation of the stimulus, phases are determined from the signs of the elements of a row of an eight-by-eight Hadamard matrix. These frequencies and phases provide for accurate measurement of the first-order frequency kernel, without interference from higher-order combination frequencies (Victor & Shapley, 1980). The analysis signal was presented with modulation depths per sinusoid m_{anal} of 0·0156, 0·0312, 0·0625 and 0·125. The root-mean-squared modulation depth of the sum-of-sinusoids signal is $2m_{\text{anal}}$; the maximum modulation depth, which is achieved only once in 65536 bins, is $8m_{\text{anal}}$.

In the synthesis episodes, the temporal modulation signal $s_{\text{syn}}(t)$ consisted of a sequence of abrupt changes between steady levels. All units were tested with a symmetrical square-wave signal, of temporal frequency $f_{\text{syn}} = 1·05$ or 0·26 Hz, with equal excursion above and below zero:

$$s_{\text{syn}}(t) = m_{\text{syn}} \, \text{sq}(f_{\text{syn}} t), \tag{3}$$

where $m_{\text{syn}}(t)$ is the modulation depth of the synthesis episode and $\text{sq}(u)$ is a symmetrical square-wave function defined by

$$\text{sq}(u) = \begin{cases} +1, & \text{if } n \leqslant u > n + \frac{1}{2} \quad \text{for some integer } n \\ -1, & \text{if } n + \frac{1}{2} \leqslant u < n + 1 \quad \text{for some integer } n. \end{cases} \tag{4}$$

The square-wave synthesis episodes were run at a range of modulation depths m_{syn} (typically 0·0625–0·5).

In other synthesis episodes, the square-wave modulation signal was replaced by a signal with a more complex sequence of levels. This sequence was of two varieties. In one variety, the temporal modulation values formed a three-level pseudo-random sequence, with values chosen with equal probability from the set $\{-m_{\text{syn}}, 0, m_{\text{syn}}\}$. In the second variety, the 'contrast-jump' experiment, the temporal modulation signal consisted of eight cycles of a symmetric square-wave at a low amplitude, $m_{\text{syn}}/4$, followed by eight cycles of a symmetric square wave at a higher amplitude, m_{syn}. In both cases, the maximum modulation depth m_{syn} was either 0·25 or 0·5, temporal modulation values changed every 118 ms, and the sequence repeated every 3·787 s (0·26 Hz).

Analysis and synthesis episodes were alternated, with 10 s in between episodes during which the display was a uniform field at the mean luminance. Modulation depths were increased by a factor of two after each analysis–synthesis pair. A block consisting of one episode of each condition at each modulation depth was repeated several (usually four) times.

Analytical methods

In order to apply the formalisms of systems analysis, we consider the output variable to be the instanteous firing rate $r(t)$, which is the probability per unit time of a nerve impulse. For simple periodic stimuli, the ordinary response histogram provides an unbiased estimate of this quantity integrated over the bin width (Brodie, Knight & Ratliff, 1978). For the sum-of-sinusoids signal, the impulse train considered as a sequence of delta functions plays the same role.

The response of a transducer to a sum-of-sinusoids input is described by a sequence of frequency kernels (Victor & Shapley, 1980). For a linear transducer, the first-order frequency kernel is essentially the transfer function scaled by the modulation depth. The frequency kernels generalize the notion of a transfer function to non-linear transducers. The first-order frequency kernel K_1 is the set of Fourier coefficients of the best linear approximation of the response $r_{\text{anal}}(t)$ to a sum-of-sinusoids signal $s_{\text{anal}}(t)$. This quantity, which depends on the input modulation depth m_{anal}, is defined at the input frequencies f_j by

$$K_1(f_j; m_{\text{anal}}) = 2 < r_{\text{anal}}(t) \exp[-i(2\pi f_j t + \phi_j)] >, \quad (5)$$

where $< >$ denotes an average over time and phase set (Victor & Shapley, 1980, and $i = \sqrt{-1}$). Because the response $r_{\text{anal}}(t)$ is considered to be a sum of delta functions, the average in eqn. (5) reduces to a trigonometric sum, with one term for each nerve impulse. Note that the first-order frequency kernel has dimensions of impulses per second, and is not normalized for input modulation depth.

The first-order frequency kernel (measured with multiple sinusoids simultaneously) and the transfer function (measured with the same sinusoidal components, but presented individually) have distinct behaviours. Consider a transducer consisting of a linear filter followed by a static non-linearity. For this transducer, the shape of the first-order frequency kernel depends only on the linear filter (Victor & Knight, 1979); the shape of the transfer function depends on both the linear filter and the static non-linearity. This distinction is crucial for the present analysis, which attempts to separate linear and non-linear phenomena in the X cell response.

RESULTS

Qualitative aspects of response dynamics

Although X cell responses are approximately linear, the dynamics of the responses show consistent deviations from strict linearity (Shapley & Victor, 1978). The purpose of the initial experiments is to distinguish between the roles of local contrast and local luminance in producing these deviations.

Responses of X cells were elicited by grating stimuli whose contrast was modulated by a symmetric square wave (eqn. (3)) of modulation depth m_{syn} (the 'standard condition'). In addition, responses to contrast appearance were measured, by using a temporal modulation signal which alternated between m_{syn} and zero (the 'up condition'), between zero and $-m_{\text{syn}}$ (the 'down condition'). These three stimuli shared an identical spatio-temporal mean luminance of L_0 (when averaged over the entire spatial stimulus). The direction and size of the stimulus transients (as a Weber fraction) were equal in the up and the down conditions. However, the time-averaged *local* luminance over the centre was smaller in the down condition ($L_0(1-m_{\text{syn}}/2)$) than in the up condition ($L_0(1+m_{\text{syn}}/2)$). The standard condition had a time-averaged local luminance of L_0, independent of modulation depth m_{syn}.

Typical responses of on-centre and off-centre X cells to high-spatial-frequency gratings are shown in Fig. 1. For the on-centre unit (Fig. 1*A*), there is an excitatory burst when the luminance over the centre increased, followed by a smaller sustained component of the response. The ratio of the size of the transient component of the response to the size of the sustained component increased with increasing modulation

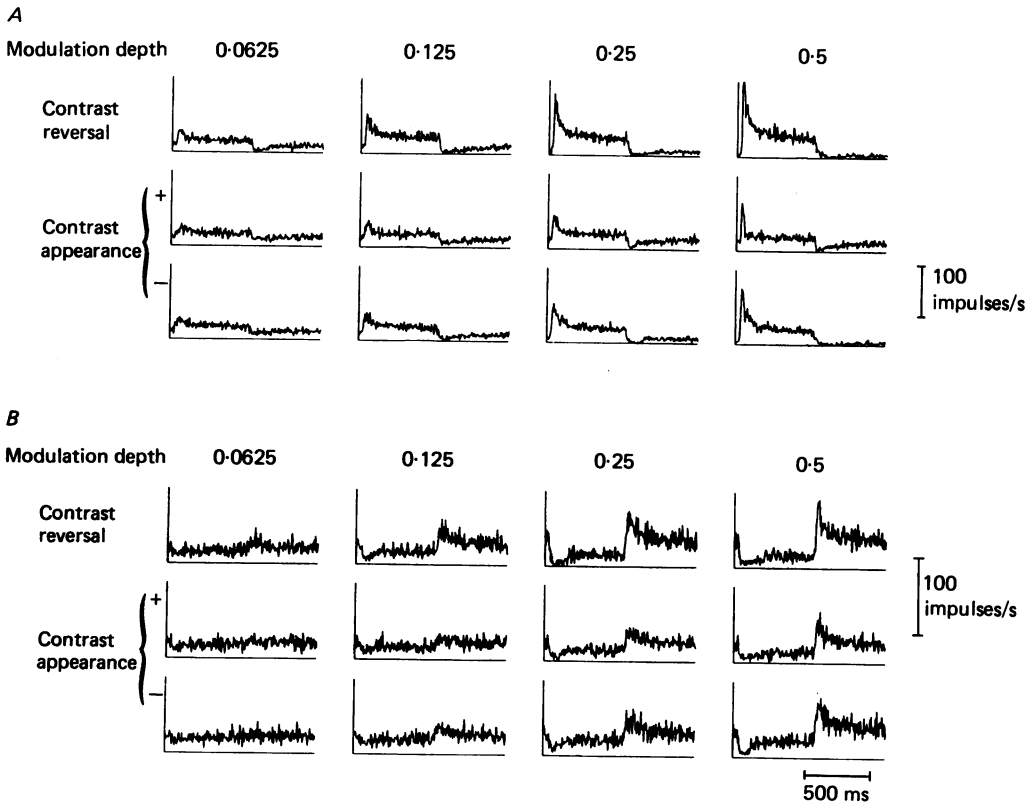

Fig. 1. Responses of retinal ganglion cells to square-wave contrast reversal and pattern appearance. *A*, unit 15/9, on-centre X cell, 1 cycle/deg grating. *B*, unit 3/1, off-centre X cell, 2 cycle/deg grating. First row: pattern reversal; second row: appearance–disappearance, with appearance phase consisting of a bright grating peak over the centre; third row: appearance–disappearance, with appearance phase consisting of a dark grating over the centre. For each column, indicated contrasts are peak stimulus contrasts. Each histogram represents four episodes of 30·3 s each (128 passes). In this and all other Figures, the bin width for spike histograms is 3·7 ms. There is no smoothing unless otherwise indicated.

depth m_{syn}. This deviation from linearity was present for all three temporal modulation patterns: greater transience was observed at greater depths of modulation, independent of whether local mean luminance remained constant (first row), increased (second row), or decreased (third row). Except for the highest contrast tested (0·5), response shape and response size depended only on the size of the transient in the modulation signal, and not on mean luminance. (The size of the stimulus transient in the standard condition was twice that of either the up or down condition at the same modulation depth m_{syn}; thus, the response to a standard square wave at a modulation depth $m_{syn} = m_0$ should be compared to the response in the up or down condition at a modulation depth $m_{syn} = 2m_0$.)

At the lowest modulation depth, the response following a local luminance decrement over the centre was approximately equal in size and opposite in shape to the response following a luminance increment. Perfect antisymmetry is not present; the

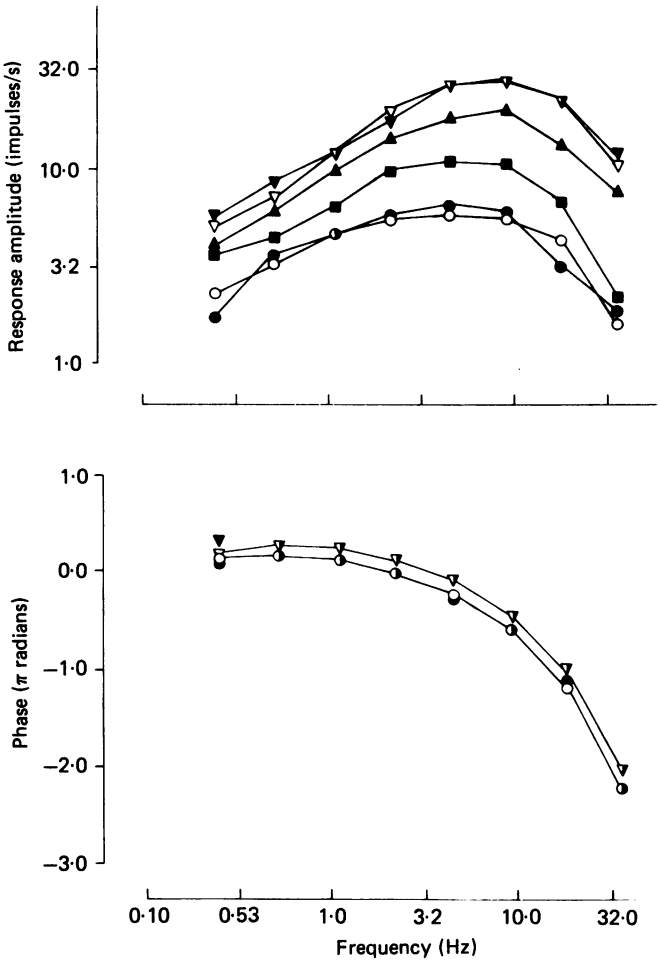

Fig. 2. First-order frequency kernels of the on-centre X cell of Fig. 1 *A* to sum-of-sinusoids modulation of a 1 cycle/deg grating at a range of modulation depths per sinusoid, m_{anal}: 0·015625 (●, ○); 0·031 25 (■); 0·0625 (▲); 0·125 (▼, ▽). Filled symbols: measured first-order frequency kernels. Open symbols: best-fitting model transduction corresponding to frequency kernels measured at low and high modulation depths. The analytic form is eqn. (6). Half-filled symbols indicate coincidence of data and model. For clarity, phase data are shown only for the lowest and highest depths of modulation.

inhibitiory transient is less prominent than the excitatory transient. The departure from antisymmetry increases as modulation depth increases.

Similar results were obtained for the off-centre unit (Fig. 1 *B*). The response grew more transient with increasing modulation depth, and did not depend on the local mean luminance falling over the centre. At lower modulation depths, approximate antisymmetry exists between excitatory (halfway through the stimulus cycle; centre luminance decreasing) and inhibitory (beginning of the stimulus cycle; centre luminance increasing) phases of the responses. At higher modulation depths, the excitatory response was more prominent than the inhibitory response. The require-

ment for a non-negative firing rate forces a departure from perfect antisymmetry; most, but not all, of the departure appears related to this requirement.

Thus, within the contrast range tested, the change in response shape appears to depend on the size of the contrast step and not on the local mean luminance over the centre. This phenomenon will be explored further below.

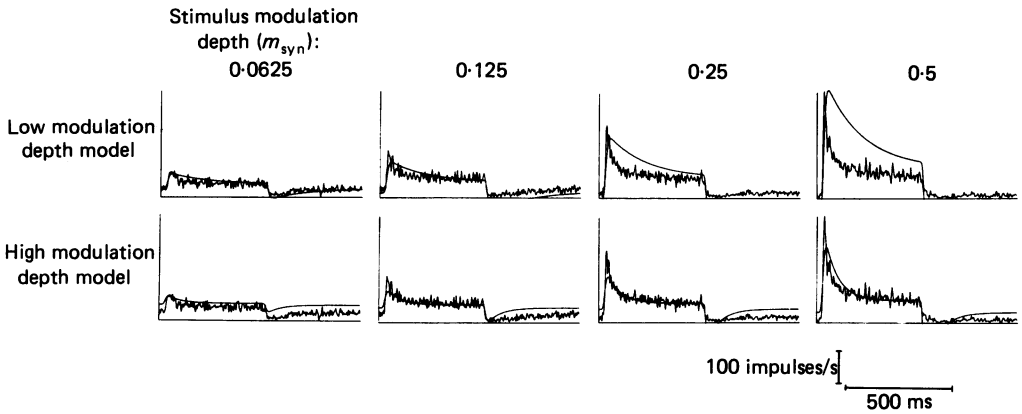

Fig. 3. Responses of an on-centre X cell to contrast reversal of a 1 cycle/deg grating at a range of modulation depths m_{syn}. In the first row, the observed step responses (irregular tracings, redrawn from Fig. 1) are compared with the prediction (smooth curve) of a linear model based on the first-order frequency kernel measured with modulation depth per sinusoid $m_{anal} = 0{\cdot}015625$. Model parameters (see text) are $A = 380$ impulses/(s.unit contrast), $M = 31$ impulses/s, $N_L = 16$, $T_L = 2{\cdot}02$ ms, $T_S = 0{\cdot}175$ s, $H_S = 0{\cdot}716$ and $D = 3$ ms. In the second row, the same observed step responses are compared with the prediction of a transfer function fitted to the first-order frequency kernel measured with a modulation depth per sinusoid $m_{anal} = 0{\cdot}125$. Model parameters are $A = 235$ impulses/(s.unit contrast), $M = 47$ impulses/s, $N_L = 16$, $T_L = 1{\cdot}82$ ms, $T_S = 0{\cdot}062$ s, $H_S = 0{\cdot}857$ and $D = 3$ ms. Unit 15/9.

Quantitative aspects of response dynamics

The aim of the next experiment is to determine what aspects of response dynamics are explained by a linear model, and what kinds of non-linearities are suggested by the deviation from linear behaviour. We begin by attempting to predict the response to stepwise modulation of a pattern from a linear model whose parameters are derived from responses to sum-of-sinusoids modulation of the same pattern.

Linear and quasi-linear modelling. Fig. 2 shows the first-order frequency kernels calculated from the response of the X cell of Fig. 1*A* to the sum-of-sinusoids signal (eqn. (2)). As modulation depth per sinusoid m_{anal} increases, the temporal frequency of best response increases. The ratio of the response at $m_{anal} = 0{\cdot}125$ (filled inverted triangles) to the response at $m_{anal} = 0{\cdot}015625$ (filled circles) increases as temporal frequency increases. This over-all shift to higher temporal frequencies at higher modulation depths is accompanied by a relative phase advance at higher modulation depths.

Fig. 3 (smooth curves) shows linear predictions of the step responses derived from the first-order frequency kernels of Fig. 2. The model predictions shown in the first row of Fig. 3 are calculated in the following fashion. An analytical transfer function

(eqn. (6), below) is fitted to the first-order frequency kernel measured at the lowest modulation depth (lower curves of Fig. 2). The step response of this model system is calculated by superposition of responses to the Fourier components of the step stimulus. The average firing rate in response to the sum-of-sinusoids signal, M, is added to this Fourier synthesis to provide the model prediction.

The model transfer function is

$$K_1(\omega/2\pi;\, m_{\text{anal}}) = \pm m_{\text{anal}}\, A \exp(-i\omega D).[1/(1+i\omega T_L)]^{N_L}.[1-H_S/(1+i\omega T_S)]. \quad (6)$$

In this equation, the initial (+) sign is chosen for on-centre units; the (−) sign for off-centre units. A is the over-all gain with dimensions of impulses per second per unit contrast, D is a conduction delay (in seconds), T_L is the time constant (in seconds) of one of N_L low-pass stages, H_S is the (dimensionless) strength of the high-pass filter and T_S is the time constant (in seconds) of the filter which forms a subtractive high-pass stage. (This transfer function is that of Shapley & Victor (1981) with $N_H = 1$ and the substitutions $H_S = k/(1+k)$ and $T_S = T_H/(1+k)$.) The conduction delay D is estimated at 3 ms from the data of Stone & Fukuda (1974). The parameters A, N_L, T_L, H_S and T_S (see Fig. 3 legend for values) were fitted to the data using a non-linear least-squares procedure as described in Shapley & Victor (1981). As determined by this procedure, the estimated value of the total low-pass delay time $N_L T_L$ is more robustly determined than the number of low-pass stages N_L or the individual time-constant T_L (Shapley & Victor, 1981); for this reason, we will usually focus on the parameter combination $N_L T_L$ rather than on the individual parameters N_L and T_L.

The analytic transfer function (6) provides an excellent description of the measured first-order frequency kernel (Fig. 2), and generates a close match to the step response measured at the lowest modulation depth (Fig. 3, upper left-hand corner). But this (and any) linear model predicts that the response will grow proportionally with modulation depth, and will not change in shape. Thus, the linear prediction of the response to a step of large modulation depth ($m_{\text{syn}} = 0{\cdot}25$ or $0{\cdot}5$) deviates substantially from the observed step response – the observed step response has a smaller sustained component, and a briefer transient, than the linear prediction (Fig. 3, upper right-hand corner).

As seen in Fig. 2, measured first-order frequency kernels do not simply scale with modulation depth; responses at high temporal frequencies grow more rapidly than do responses at low temporal frequencies. As seen in Fig. 3, the step responses also indicate that the centre dynamics become more transient when the modulation depth is higher. If the dynamics are effectively linear except for a parametric dependence on modulation depth, step responses should be modelled accurately from the transfer function fitted to the first-order frequency kernel measured at a similar average modulation depth. This is the hypothesis of the quasi-linear model. In physiological terms, we posit a neural measure of contrast, which is sensitive to fractional deviations of luminance from its mean over some region of space and time. This neural measure of contrast acts to tune the centre dynamics. The quasi-linear model assumes that the neural measure of contrast varies slowly in comparison with the other timescales of centre dynamics, and that for each stimulus, it may be regarded as a constant parameter. The quasi-linear model is tested in the second row of Fig. 3.

In the second row of Fig. 3, the same observed step responses are compared with a Fourier synthesis generated from the first-order frequency kernel at the highest modulation depth ($m_{anal} = 0{\cdot}125$ per sinusoid). This broad-band signal has the same root-mean-squared modulation depth as does the step of modulation depth $m_{syn} = 0{\cdot}25$. The corresponding first-order frequency kernel predicts a more transient step response than does the first-order frequency kernel measured at the lower modulation depths. Although agreement with the measured step responses at the contrasts of 0·25 and 0·5 is improved, the observed step responses are still more transient than the prediction of the quasi-linear model. As expected, this model provides a poor prediction of the response to a step of low modulation depth (Fig. 3, lower left-hand corner): the predicted response has a smaller sustained/transient ratio than the actual response, and the mean firing rate in response to the step is smaller than predicted from the sum-of-sinusoids signal.

Dependence of modal parameters on contrast. The deviations of responses predicted by the quasi-linear model from the actual step responses (Fig. 3) were consistent from cell to cell. This suggests that the main assumption of the quasi-linear model – that the neural measure of contrast may be regarded as a constant over the stimulus period – is only approximately correct, and needs modification. We proceed to make this modification. First, we will separate model dynamics into contrast-dependent and contrast-independent components. Then, we will allow the contrast-dependent components to vary with time, as governed by a neural measure of contrast. The resulting model will account for the discrepancies exemplified by Fig. 3.

At any given modulation depth, the analytic transfer function (6) provides an accurate description of the measured first-order frequency kernel (Fig. 2). Thus, the change in the parameters that provide the best-fitting transfer function (6) at each modulation depth characterizes the change in ganglion cell centre dynamics with contrast. Remarkably, the only dynamical parameter which shows a consistent and marked contrast dependence is the high-pass constant T_S. The remaining parameters either do not show a consistent change (N_L T_L and H_S) or change in a fashion which is predicted in large part by the truncation non-linearity (A and M). This is illustrated in Fig. 4.

Data from the on-centre X cell of Fig. 1A – 3 are presented in Fig. 4*A*. The gain A decreases by approximately 38% at high contrasts; there is a comparable increase in the mean firing rate M. Most of this change (open circles) is accounted for by the truncation required by a non-negative firing rate (Appendix). The low-pass delay $N_L T_L$ is constant to within 10% as contrast varies. The high-pass strength H_S increases by approximately 20% as contrast increases. The remaining dynamical parameter, the high-pass time constant T_S, changes by a factor of three as contrast increases. The on-centre X cell of Fig. 4*B* has a somewhat smaller gain, and a smaller increase in mean rate as contrast increases. Nevertheless, as contrast increases, a fourfold decrease in the high-pass time constant T_S is observed. The on-centre X cell of Fig. 4*C* is unusual in that the decrease in gain, A, is greater than that expected from simple truncation. The remaining parameters behave in a similar fashion as in the other X cells.

Data from three off-centre X cells are presented in Fig. 4*D*, *E* and *F*. The units of Fig. 4*D* and *E* have a non-zero maintained discharge. For these units, the

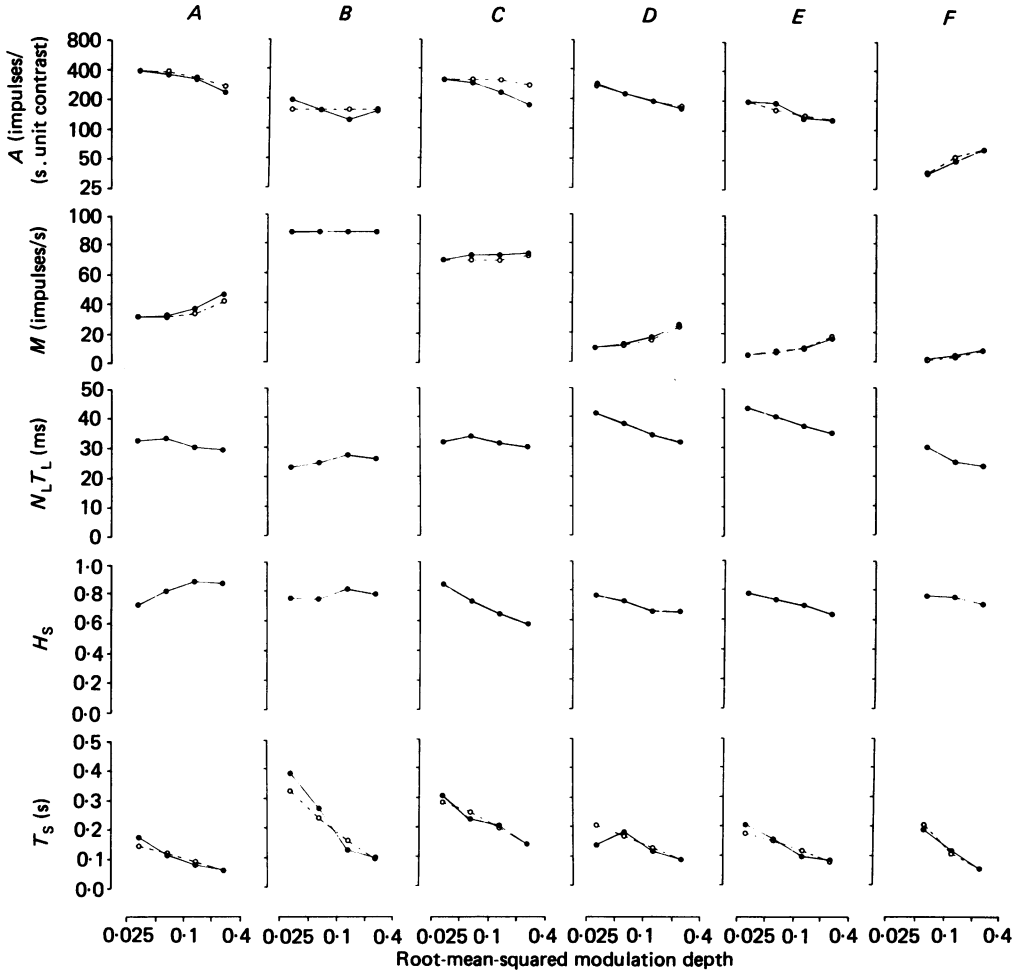

Fig. 4. ●: the dependence of the parameters of the quasi-linear model on modulation depth. The parameters, A, N_L T_L, H_S, and T_S were obtained by fitting the model transfer function (6) to the measured first-order frequency kernel. M is the average firing rate in response to the sum-of-sinusoids stimulus. The abscissa, root-mean-squared modulation depth, is equal to twice the modulation depth of each sinusoid in the sinusoidal-sum stimulus. ○: fits to the data assuming that the only non-linearities are the truncation at 0 impulses/s of impulse generation (Appendix), and the dependence of T_S on contrast given by eqns. (7) and (8). A, on-centre X cell unit 15/9, 1·0 cycle/deg grating. B, on-centre X cell unit 18/8, 1·5 cycle/deg grating. C, on-centre X cell unit 12/2, 1·5 cycle/deg grating. D, off-centre X cell unit 10/8, 1·0 cycle/deg grating. E, off-centre X cell unit 12/5, 30 min central spot. F, off-centre X cell unit 8/14, 0·5 cycle/deg grating.

dependence of the dynamical parameters on contrast is similar to that of the on-centre units. The data of Fig. 4E were obtained from a 30 min-of-arc-diameter central spot, rather than a grating, and thus demonstrate that the change in dynamics does not require patterned stimulation of the surround. The unit of Fig. 4F was typical of X cells that have no maintained discharge in the absence of stimulation. In this unit, both gain A and mean firing rate M increase with increasing contrast. Such behaviour

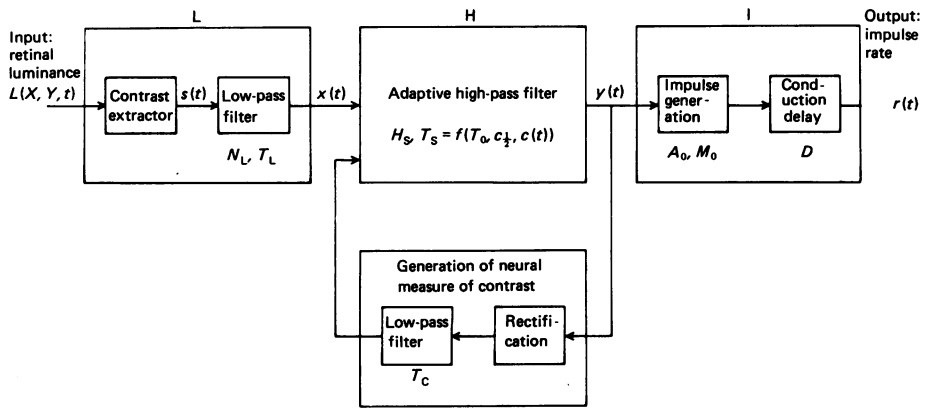

Fig. 5. A diagram of the model for centre dynamics. The model consists of a low-pass stage (L), followed by an adaptive high-pass stage (H), and an impulse-generating stage (I). Components of the model are defined in detail in the text and Table 1.

TABLE 1. The dynamical model

	Time domain (non-linear)	Frequency domain (linearized)
	Low-pass filter (L)	
(L1)	$x(t) = \pm \int_0^\infty \frac{s(t-t')}{N_L!} (t'/T_L)^{N_L-1} e^{-t'/T_L} dt'$	$\tilde{x}(\omega) = \pm(1+i\omega T_L)^{N_L} \tilde{s}(\omega)$
	High-pass filter (H)	
(H1)	$T_S(t)\dot{y}(t) = -y(t)+T_S(t)\dot{x}(t) + (1-H_S)x(t)$	$\tilde{y}(\omega) = [1-H_S/(1+i\omega T_S)]\tilde{x}(\omega)$
(H2)	$T_S(t) = T_0/(1+c(t)/c_{\frac{1}{2}})$	
(H3)	$T_C \dot{c}(t) = \lvert y(t)\rvert - c(t)$	
	Impulse generation (I)	
(I1)	$r(t) = \max(A_0 y(t-D)+M_0, 0)$	$\tilde{r}(\omega) = A_0 e^{-i\omega D}\tilde{y}(\omega) + M_0\delta(0)$

Summary of a non-linear model for the dynamics of the X cell centre. The input to the model is $s(t)$, the signed Weber contrast at the centre. The low-pass filter L is comprised of N_L stages of time constant T_L (eqn. (L1)). The low-pass filter is linear and is equivalently described in either the time or the frequency domain. The initial (+) sign is used for on-centre cells; the (−) sign for off-centre cells. The output of the low-pass filter, $x(t)$, is the input to a high-pass filter H. The linearized dynamics of this filter (eqn. (H1)) correspond to a substractive high-pass stage of strength H_S and time constant T_S. The effective time constant of this high-pass stage is postulated to depend on contrast, $c(t)$ according to eqn. (H2). The neural measure of contrast $c(t)$ is a low-pass transformation (time constant T_C) of the absolute value of the output of this high-pass stage, $y(t)$ (eqn. (H3)). The time derivatives of $x(t)$, $y(t)$ and $c(t)$ are denoted $\dot{x}(t)$, $\dot{y}(t)$ and $\dot{c}(t)$. Eqns. (H1)–(H3) cannot be expressed simply in the frequency domain because of their non-linearities. The firing rate $r(t)$ is the sum of the output high-pass stage scaled by an over-all gain A_0, and the firing rate in the absence of stimulation, M_0. It is delayed by a conduction delay D and must be non-negative (eqn. (I1)). The frequency domain representation neglects the truncation at 0 impulses/s.

is predicted by a simple threshold non-linearity at the point of impulse generation (undriven mean firing rate $M_0 < 0$ in the Appendix). A quantitative comparison of the observed gain and mean firing rate with the consequences of this non-linearity is provided by the open circles, which are calculated from the analysis of the Appendix with $M_0 = -5$ impulses/s and $A_0 = 152$ impulses/(s.unit contrast). In all other respects, the dependence of the dynamical parameters of this unit on contrast was typical of the other on- and off-centre units, as described above.

In summary, the quasi-linear model may be decomposed into three parts (Fig. 5; Table 1). The initial stage is a low-pass filter which transforms the Weber fraction

$s(t)$ to $x(t)$. This stage, whose parameters are N_L and T_L, appears to be strictly linear. The second stage is a high-pass filter, which transforms $x(t)$ into a signal $y(t)$. This stage, whose parameters are H_S and T_S, depends parametrically on contrast. Finally, the signal $y(t)$ is added to an offset M_0 and drives a spike-generating mechanism whose intrinsic gain is A_0. The lag time between impulse generation and their detection in the response $r(t)$ is the conduction delay D.

Dynamic non-linear models. The data of Fig. 4 suggest that the dependence of dynamics on modulation depth is due primarily to the dependence of the high-pass time constant T_S on contrast; the dependence of gain and mean firing-rate on modulation depth is due primarily to the intrinsic non-negativity of the impulse rate. In Fig. 3, we saw that the quasi-linear hypothesis (a slowly varying neural measure of contrast) was only approximately correct. We now extend the quasi-linear model to a dynamic non-linear model, in which a time-varying neural measure of contrast, denoted $c(t)$, adjusts the high-pass time constant T_S in a dynamic fashion. This dynamic non-linear model will be tested by its ability to predict responses to a series of analysis stimuli. The first step in this procedure is to unify the several quasi-linear models determined at each modulation depth into a single model.

As seen from the sum-of-sinusoids experiments summarized in Fig. 4, T_S decreases as contrast increases, and the change in T_S persists to the lowest modulation depths at which parameters can be reliably measured. Empirically, the measured values $1/T_S$ are a linear function of modulation depth. Thus, the relationship of T_S to contrast is described by two parameters: the extrapolated value of T_S at a modulation depth of zero, denoted T_0, and the value of the internal contrast signal $c(t)$ at which T_S is halved, denoted $c_{\frac{1}{2}}$.

To determine the parameters T_0 and $c_{\frac{1}{2}}$, it is necessary to specify the details of the dependence of the neural measure of contrast $c(t)$ on the input signal, and to compare quasi-linear dynamics measured at several modulation depths. It is postulated (see Discussion) that the neural measure of contrast $c(t)$ is derived from the *output* of the centre dynamics, denoted $y(t)$. The relationship of $c(t)$ to $y(t)$ must be even-order, since contrast (by definition) is independent of the direction of deviation from the mean luminance.

The simplest even-order non-linearity is a quadratic transformation. If the coupling of $c(t)$ to $y(t)$ were quadratic, then the dependence of the dynamical parameters on contrast would asymptotically vanish at small depths of modulation. However, the dependence of T_S on contrast typically *does not* become negligible as depth of modulation decreases (Fig. 4, bottom row), so a quadratic coupling is excluded. A similar argument excludes any transformation which is analytic (smooth) near zero; thus, the transformation from $y(t)$ to $c(t)$ appears to have a singularity near $y(t) = 0$. In view of the approximately linear relationship between $1/T_S$ and modulation depth, this singularity is similar to that of a rectifier, and we postulate that $c(t)$ depends on the rectified centre output, $|y(t)|$.

In the quasi-linear regime, the value of the contrast signal $c(t)$ in response to any given stimulus is assumed to be constant and equal to the average, rectified value of $y(t)$ in response to the same stimulus. In this regime, $y(t)$ may be computed from the input signal $s(t)$ in the frequency domain by

$$\tilde{y}(\omega) = \pm \tilde{s}(\omega)\,[1/1 + i\omega T_L)]^{N_L}\,[1 - H_S/(1 + i\omega T_S)]. \tag{7}$$

(This follows by combining eqns. (L1) and (H1) of Table 1.) We determine the parameters T_0 and $c_{\frac{1}{2}}$ by comparing quasi-linear dynamics measured at several modulation depths. The parameters are determined by a least-squares fit to

$$1/T_S = (1/T_0)\,(1 + < |\,y(t)\,| > /c_{\frac{1}{2}}), \tag{8}$$

with $y(t)$ given by eqn. (7). Here, we have formalized the notion that $1/T_S$ is a linear function of the neural measure of contrast $c(t)$, and that $c(t)$ is held constant at its average value $< |\,y(t)\,| >$. Eqns. (7) and (8) provide the fits for T_S shown as open circles in Fig. 4.

Now that quasi-linear dynamics at several modulations depths have been modelled in a unified fashion, the quasi-linear model may be converted into a dynamic non-linear model. To do this, the quasi-linear approximation to the contrast signal used in eqn. (8), $< |\,y(t)\,| >$, is replaced by a time-varying signal $c(t)$. As a consequence, the high-pass time constant T_S is now time-varying as well (Table 1, eqn. (H2)).

The dynamics of the neural contrast signal $c(t)$ must be embodied in a relationship between $c(t)$ and $y(t)$. The general success of the quasi-linear model suggests that $c(t)$ should preserve the low-frequency components of $|\,y(t)\,|$. Victor (1985) explored relationships between $c(t)$ and $|\,y(t)\,|$ consisting of single and multiple low-pass filters with a range of time constants T_C. Long time constants (greater than 100 ms) provided model predictions that were very similar to that of the quasi-linear model. Time constants of 50 ms or less improved the fit to simple step responses; the best fit was obtained with a single low-pass stage of time constant T_c in the range of 15 ms. Alternative values of T_C in the range of 5 to 25 ms provided model predictions that would not be experimentally distinguishable from the predictions with $T_C = 15$ ms. For this reason, a single low-pass stage of time constant $T_C = 15$ ms is chosen to relate the neural contrast signal $c(t)$ to $|\,y(t)\,|$ (eqn. (H3) of Table 1).

Tests of the dynamic non-linear model. For each X cell, parameters of the dynamic non-linear model were extracted from responses to sum-of-sinusoids modulation of a spot or grating, as described above. Then, the dynamic non-linear model (Table 1) was used to calculate responses to step modulation of the same spatial pattern. (For this purpose, the non-linear system of eqns. (H1–H3) was integrated numerically.) This procedure also yielded a theoretical curve for the neural measure of contrast $c(t)$. Results of this calculation for the on-centre X cell of Fig. 1*A*–3 are shown in Fig. 6. The non-linear model provides an excellent description of the dynamics of the step response across the entire modulation depth tested. In particular, the model accounts for the transience of the measured high-contrast responses, and explains the deviations of the quasi-linear model from the actual response (Fig. 3).

The reason that the non-linear model provides for more transient responses than the linear or quasi-linear models is the sharp peak of the neural measure of contrast $c(t)$ at each stimulus transient. The value of the high-pass time constant T_S decreases when the instantaneous value of $c(t)$ increases (eqn. (H2) of Table 1). In the quasi-linear model, which is equivalent to a long T_C (> 100 ms), the peak of $c(t)$ is smoothed out over time. The effect of the peak of $c(t)$ is that just after each transient, the instantaneous effective high-pass time constant $T_S(t)$ is shorter than the value predicted by the quasi-linear model.

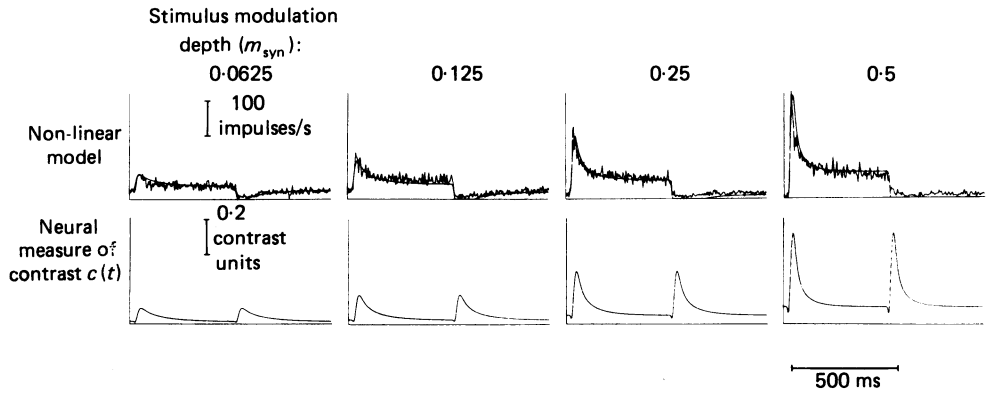

Fig. 6. Non-linear modelling of step responses of an on-centre X cell to contrast reversal of a 1 cycle/deg grating. In the first row, the observed step responses (irregular tracings, reproduced from Fig. 1) are compared with the prediction (smooth curve) of the non-linear model of Table 1 over a range of modulation depths m_{syn}. In the second row, the theoretical behaviour of the neural measure of contrast $c(t)$ is shown. Model parameters are $A_0 = 440$ impulses/(s.unit contrast), $M_0 = 31$ impulses/s. $N_L = 16$. $T_L = 1{\cdot}94$ ms, $T_0 = 0{\cdot}193$ s, $c_{\frac{1}{2}} = 0{\cdot}054$, $H_S = 0{\cdot}806$, $D = 3$ ms and $T_C = 15$ ms. Unit 15/9.

Another feature of the theoretical curve for $c(t)$ is its brief downward transient immediately before the more prominent upward rise that occurs just after each phase of contrast reversal. This downward transient is due to the fact that $c(t)$ is a low-pass filtered copy of $|y(t)|$, and $|y(t)|$ achieves its minimum value of 0 shortly after each phase of contrast reversal. This brief downward transient of $c(t)$ is irrelevant to the predictive success of the model.

More complex temporal stimulus patterns provided further tests of the non-linear model. Fig. 7 shows a comparison of measured responses with model responses for an off-centre X cell stimulated by a 1·0 cycle/deg grating modulated by the contrast-jump stimulus; Fig. 8 shows a similar comparison for the three-level pseudo-random stimulus. In both cases, the non-linear model captures the features of the actual response.

Thus, the discrepancy between the observed step response and the predicted step response of the quasi-linear model (Fig. 3) is eliminated by allowing the high-pass time constant T_S to vary with time in a natural way (Fig. 6). Furthermore, this dynamic non-linear model accurately predicts the response to more complex stimuli as well (Figs. 7 and 8).

Population aspects

As seen in Fig. 4, there is considerable variability in the values of some dynamical parameters across the cell population studied. One possible source of this variability is examined in Table 2, in which the statistics of the on-centre and off-centre units are compared. As expected, the mean firing rate is substantially lower in off-centre units than in on-centre cells. Although the most sensitive units (highest gain) are the on-centre units, there is substantial overlap of on- and off-units, and no statistically significant (Table 2) difference. The tabulated values of absolute gain A_0 take into account the analysis of truncation given in the Appendix. Off-centre X cells with no

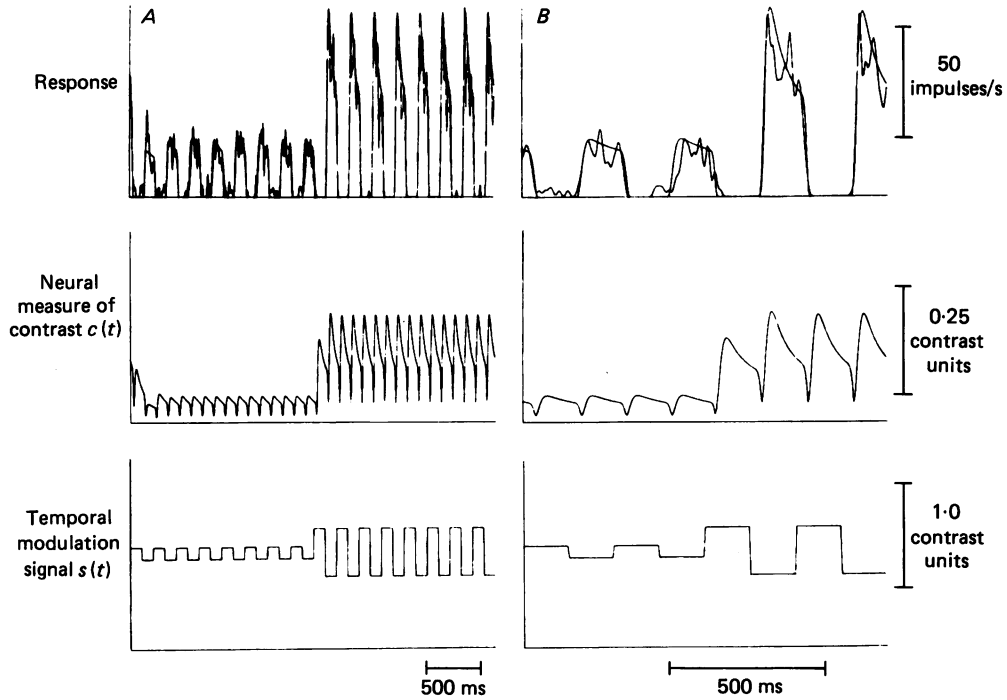

Fig. 7. Non-linear modelling of responses of an off-centre X cell to modulation of a 1·0 cycle/deg grating by a contrast-jump stimulus. *A*, the full stimulus cycle. *B*, the middle one-quarter of the stimulus cycle enlarged for detail. In the first row of each part, the observed responses (irregular tracings) are compared with the prediction (smooth curve) of the non-linear model of Table 1. Response histograms have been smoothed by a bell of half-width 3·7 ms. In the second row, the theoretical behaviour of the neural measure of contrast $c(t)$ is shown. In the third row, the temporal modulation signal is shown. Model parameters are $A_0 = 290$ impulses/(s.unit contrast), $M_0 = 10$ impulses/s, $N_L = 15$, $T_L = 2{\cdot}18$ ms, $T_0 = 0{\cdot}251$ s, $c_{\frac{1}{2}} = 0{\cdot}068$, $H_S = 0{\cdot}651$, $D = 5$ ms and $T_C = 15$ ms. Unit 10/8.

maintained discharge will have a *smaller* apparent gain at low modulation depths than at high modulation depths, while the typical on-centre unit will have a *larger* apparent gain at low modulation depths than at high modulation depths.

Values of the low-pass delay $N_L T_L$ are tightly clustered about an average value of 33 ms (coefficient of variation = 0·16). There is a slight prolongation of its average value in the off-centre units. Similarly, there is a slight decrease in the number of low-pass stages N_L in the off-centre units.

Although these differences are statistically significant (Table 2), they are unlikely to represent a difference in intrinsic dynamics of on- and off-units. Ganglion cell activity is transmitted by a stream of nerve impulses, and if the mean rate is low, there is (on average) a greater delay between a change in membrane voltage and the encoding of this change into an alteration of the firing rate. The 5 ms difference in $N_L T_L$ between on- and off-type units is easily accounted for by such a mechanism. The estimate of N_L depends critically on the estimate of responses at the highest temporal frequencies. Estimates of response amplitudes are biased upward by the presence of noise. The lower firing rate in off-units certainly changes the spectral distribution of the noise in the impulse train. The lower value of N_L in off-centre units is likely to be a consequence of relatively greater impulse-train noise in the frequency band 15–30 Hz upon which estimates of N_L depend.

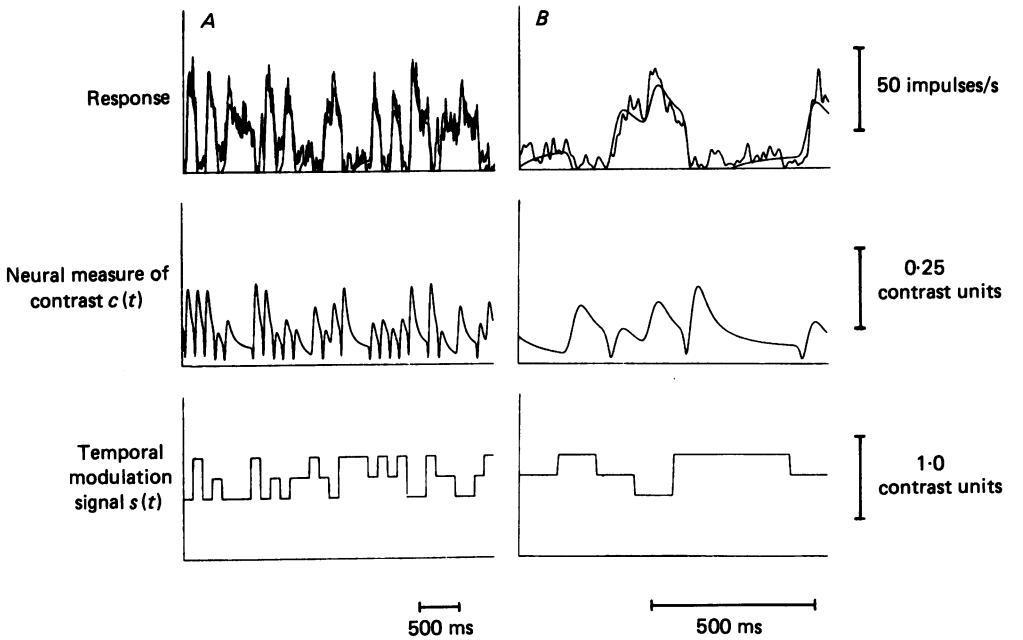

Fig. 8. Non-linear modelling of responses of an off-centre X cell to modulation of a 1·0 cycle/deg grating by a three-level pseudo-random stimulus. *A*, the full stimulus cycle. *B*, the middle one-quarter of the stimulus cycle enlarged for detail. In the first row of each part, the observed responses (irregular tracings) are compared with the prediction (smooth curve) of the non-linear model of Table 1. Response histograms have been smoothed by a bell of half-width 3·7 ms. In the second row, the theoretical behaviour of the neural measure of contrast $c(t)$ is shown. In the third row, the temporal modulation signal is shown. Model parameters are $A_0 = 176$ impulses/(s.unit contrast), $M_0 = 16$ impulses/s, $N_L = 8$, $T_L = 6{\cdot}16$ ms, $T_0 = 0{\cdot}596$ s, $c_{\frac{1}{2}} = 0{\cdot}016$, $H_S = 0{\cdot}812$, $D = 5$ ms and $T_C = 15$ ms. Unit 7/3.

The mean rate and parameters whose measured values are likely to depend on the mean rate are systematically different in on- and off-type units. The other dynamical parameters (absolute gain and descriptors of the high-pass transduction) have similar values in on- and off-type units. The total high-pass strength H_S is relatively constant across the X cell population (coefficient of variation = 0·13). Other high-pass parameters (T_0 and $c_{\frac{1}{2}}$) show wide variability across the X cell population.

The variability of parameter values across the entire population persists after segregating more central and more peripheral units, and parameter values do not depend on eccentricity. In addition, no consistent dependence of parameters on azimuth or retinal hemifield (nasal *vs.* temporal) was found. Thus, although subtle trends may not be evident in the relatively small population studied, ganglion cells with a range of dynamical parameters are represented at any retinal location.

Table 2. Population statistics for model parameters

Parameter	X cell population	Minimum	Maximum	Median	Mean	S.D.	C.V.	P
A_0 (impulses/ (s.unit contrast))	On	72·0	675·0	157·0	230·0	163·0	0·71	
	Off	22·0	290·0	164·0	160·0	78·0	0·49	> 0·1
	All	22·0	675·0	157·0	210·0	146·0	0·70	
M_0 (impulses/s)	On	22·0	99·0	71·0	70·0	21·0	0·30	
	Off	−8·8	23·0	5·0	6·0	10·0	1·80	< 0·001
	All	−8·0	99·0	66·0	51·0	35·0	0·69	
$N_L T_L$ (ms)	On	25·1	40·8	31·2	31·4	4·0	0·13	
	Off	25·9	49·2	35·3	36·1	6·9	0·19	0·028
	All	25·1	49·2	31·5	32·8	5·4	0·16	
N_L (dimensionless)	On	10	30	20	22·0	6·0	0·29	
	Off	8	20	16	15·0	5·0	0·35	0·013
	All	8	30	20	19·0	7·0	0·34	
H_S (dimensionless)	On	0·47	0·86	0·69	0·68	0·09	0·14	
	Off	0·65	0·86	0·72	0·74	0·07	0·09	> 0·1
	All	0·47	0·86	0·71	0·70	0·09	0·13	
T_0 (s)	On	0·08	1·98	0·23	0·43	0·45	1·03	
	Off	0·05	6·56	0·23	1·02	2·24	2·19	> 0·1
	All	0·05	6·56	0·23	0·61	1·25	2·06	
$c_{\frac{1}{2}}$ (unit contrast)	On	0·005	0·288	0·054	0·086	0·079	0·92	
	Off	0·001	0·535	0·078	0·150	0·189	1·26	> 0·1
	All	0·001	0·535	0·063	0·105	0·122	1·16	
D (ms)	On	3·0	6·0	4·5	4·4	1·0	0·23	
	Off	3·5	6·0	4·7	4·5	0·9	0·19	> 0·1
	All	3·0	6·0	4·5	4·4	0·9	0·21	

Population statistics for the parameters of a non-linear model for the dynamics of the X cell centre. The meaning of the parameters is defined in the text and Table 1. S.D.: standard deviation; C.V.: coefficient of variation (standard deviation/mean). Probability values for the significance of the difference of mean population statistics for on- and off-centre X cells were calculated by a bootstrap analysis of variance (Efron, 1980).

DISCUSSION

A summary of the dynamical model

The structure of the proposed model (Fig. 5) is motivated by two concepts: (1) the X cell transduction from the light stimulus to the impulse rate is at least approximately linear (Rodieck, 1965; Enroth-Cugell & Robson, 1966), and (2) over-all stimulus contrast exerts a modulatory effect on the approximately linear dynamics (Shapley & Victor, 1978).

The first stage of the model ('L' in Fig. 5) has as its input the retinal luminance $L(X, Y, t)$. The output of this stage is a low-pass transformation of luminance fluctuations, which is denoted $x(t)$. Within this first stage, a preliminary transformation extracts the signed Weber fraction $s(t)$ from the input spatio-temporal luminance pattern. Then, the signed Weber fraction $s(t)$ is transformed into $x(t)$ via a cascade of N_L low-pass filters of time constant T_L. This transduction from $s(t)$ to $x(t)$ is postulated to be strictly linear.

The preliminary extraction of a Weber fraction is postulated for several reasons. In the range of luminance fluctuations tested, the deviation of the local mean luminance from its spatio-temporal average controls the shape of the response; the local mean luminance itself does not appear to be important (Fig. 1). In all experiments here, the spatio-temporal mean of the luminance is held constant at $L_0 = 100$ cd/m^2. Normalization of the input by L_0, which converts it to a Weber

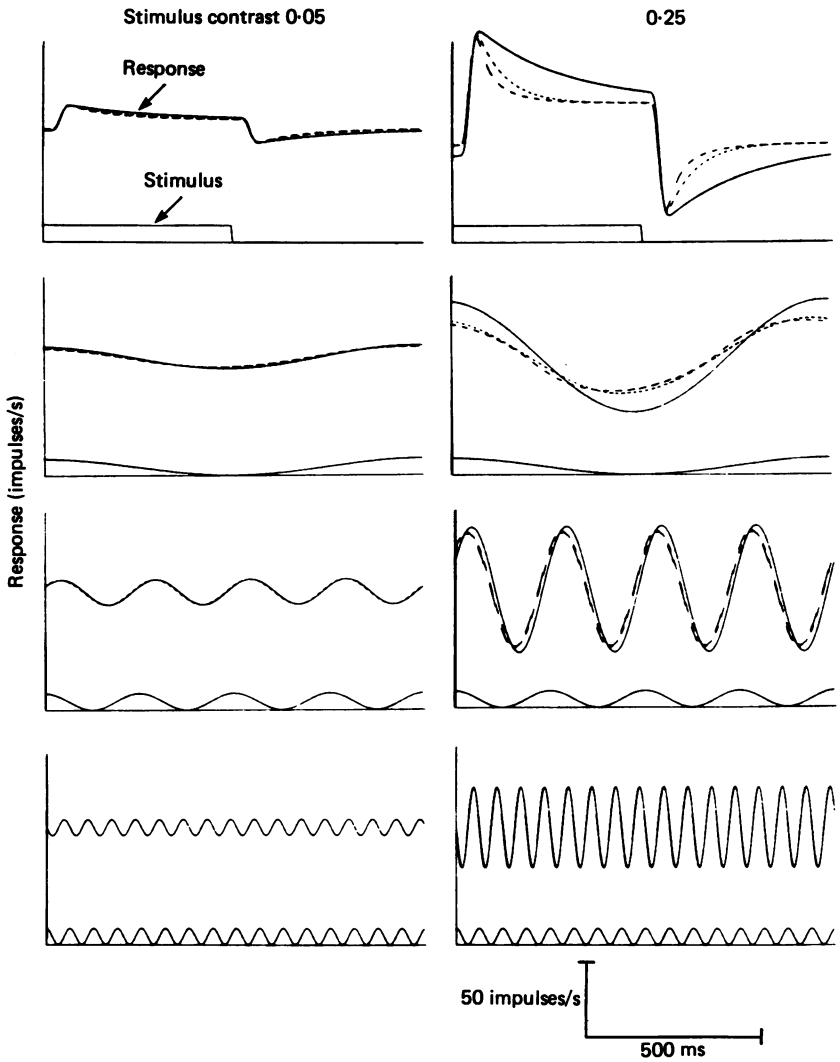

Fig. 9. Model responses of a 'typical' on-centre X cell to step and sinusoidal contrast-modulation. The model parameters are those of the median of the on-centre X cell population as given in Table 2. In each panel, the long dashed lines represent the responses of the full (dynamic) non-linear model of Table 2, with $T_C = 15$ ms. The short dashed lines represent the responses of the quasi-linear model, which is a limiting case of the non-linear model for $T_C \to \infty$. The continuous lines represent the responses of the strictly linear model, which is a limiting case of the quasi-linear model for $c_1 \to \infty$. The temporal modulation signal is shown under each set of model responses; modulation depth is 0·05 (first column) and 0·25 (second column). At the low modulation depths, responses of the three models nearly superimpose. At high modulation depths, low temporal frequencies are suppressed in the quasi-linear model, and to a somewhat greater extent in the full non-linear model.

fraction, removes a dimensional constant from the modelling. This normalization also recognizes the presence of a Weber's law mechanism in the earliest stages of visual processing (Baylor & Hodgkin, 1974).

The second stage of the model ('H' in Fig. 5) is an adaptive high-pass transduction, and incorporates the contrast gain control (Shapley & Victor, 1981). The input to this stage is $x(t)$; the output is denoted $y(t)$, which is a bandpass-filtered transformation to the original input $L(X, Y, t)$. At this stage, the neural measure of contrast $c(t)$ exerts its effects on dynamics. If the neural measure of contrast $c(t)$ is held fixed at a constant value $c(t) = c$, then the transduction from $x(t)$ to $y(t)$ is a single, strictly linear high-pass stage of strength H_S and time constant $T_S = T_0/(1+c/c_{\frac{1}{2}})$. If the neural measure of contrast $c(t)$ is allowed to vary dynamically, the effective high-pass time constant T_S varies dynamically as well. This adaptive high-pass transduction is conveniently expressed in the time domain (eqn. (H1) of Table 1; derived in Victor (1985)). With increasing values of the neural contrast signal $c(t)$, the effective high-pass time constant T_S decreases (eqn. (H2) of Table 1). The parameter $c_{\frac{1}{2}}$ indicates the contrast at which T_S falls to one-half of its extrapolated value T_0 at a contrast of 0; $c_{\frac{1}{2}}$ is typically 0·1 or less.

The time constant T_C indicates how rapidly the neural measure of contrast fluctuates (eqn. (H3) of Table 1). If T_C were long (100 ms or more), then the dynamically adjusting model's behaviour would approach that of a quasi-linear model. The shortness of T_C (15 ms) indicates that contrast adjusts retinal dynamics essentially immediately. The generation of the neural measure of contrast $c(t)$ will be discussed more fully below.

The final stage of the model ('I' in Fig. 5) is the transduction from the bandpass-filtered input signal $y(t)$ to the impulse rate $r(t)$. This stage consists of multiplication of the signal $y(t)$ by an absolute gain A_0 and conversion to a firing rate. The conversion to a firing rate is assumed to be linear except for an offset equal to the mean firing rate M_0. For the purposes of comparison of the model to responses measured along the optic tract, a conduction delay D is included.

The neural measure of contrast. Several lines of evidence place constraints on the network that provides the neural measure of contrast $c(t)$. The neural measure of contrast depends on the fractional excursion of luminance at a given point and time from its mean value, and not on the direction of this excursion. Thus, neural contrast is an *even* function of the (signed) Weber fraction $s(t)$. However, if stimulus contrast $s(t)$ were coupled to the dynamical parameters through a quadratic non-linearity, then the dependence of the dynamical parameters on modulation depth would become negligible at low modulation depths. As seen in Fig. 4, the effect of stimulus contrast on the apparent high-pass time constant T_S persists to the lowest modulation depths at which responses can be reliably determined. This implies that a rectifier, or some other non-linearity with a similar even singularity at zero, is involved in the generation of $c(t)$.

Previous experiments (Shapley & Victor, 1978, 1979) have shown that the contrast network has both low- and high-pass temporal tuning. For fine patterns, the optimum flicker frequency for induction of contrast gain control effects is 4–8 Hz. This must indicate temporal tuning of a filter prior to the rectification. This tuning is similar to the tuning of X cell centre dynamics themselves. For this reason (and with

parsimony in mind) we consider the neural measure of contrast to be derived from the bandpass-filtered input $y(t)$, rather than from the (signed) Weber fraction $s(t)$ or its low-pass tranformation $x(t)$.

Note that this postulate is quite consistent with the hypothesis that the contrast signal (which includes spatial summation of many locally rectified signals) is generated by the Y cell non-linear network (Shapley & Victor, 1980). To a first approximation, the Y cell receptive field can be thought of as an array of subunits whose outputs are rectified and summed (Hochstein & Shapley, 1976*b*; Victor & Shapley, 1979). The subunits have centre–surround organization and dynamics that resemble those of the X cell. Thus, at high spatial frequencies, a contrast signal generated by the Y cell network would be expected to resemble a rectified X cell centre response. The spatial spread of the contrast signal consequent to this array of non-linear subunits need not be considered explicitly in a formal model of the response to a spatially homogeneous stimulus, such as a grating.

Intrinsic ambiguities of input–output analysis. The model proposed is among the simplest dynamical models that account for the transient responses and the sum-of-sinusoids responses of the centre mechanism. It accurately reproduces the responses to contrast reversal (Fig. 6), a regular sequence of steps with two time scales and a large dynamic range (Fig. 7), and a pseudo-random sequence of steps (Fig. 8). In order to be relatively concise, the model makes some simplifying assumptions. Although more complex non-linearities of impulse generation may well be involved, they do not appear to be significant in determining responses to stimuli of moderate contrast. It is unlikely that all of the low-pass stages have identical time constants, that light adaptation does not affect dynamics, or that the contrast gain control has absolutely no effect on parameters other than T_S.

The experimental data also admit some flexibility for modelling the adjustment of T_S with contrast. Formally, the dynamics of the contrast gain control is at least a third-order non-linearity. Altough one might hope to analyse this coupling from third-order frequency kernels, numerical simulations show that third-order kernels are relatively insensitive to the dynamics of the coupling. An alternative approach (Victor, 1985) amounts to testing alternative ways of grafting dynamics onto eqns. (7) and (8). The result is a minimal model of the coupling: the non-linear feed-back signal is modelled as the rectified centre output filtered by a single low-pass stage with a time constant T_C of at most 15 ms. A substantially longer time constant T_C, or a multistage cascade, is inconsistent with the experimental data. However, T_C is so short in comparison with $N_L T_L$ and T_0 that the limiting case of $T_C = 0$ is not an unreasonable approximation. In this regime, the differential equation governing $c(t)$ (Table 1, eqn. (H3)) is replaced by $c(t) = |y(t)|$. The resulting system has dynamics that are for all practical purposes indistinguishable from those of the original model. Another variation on the model that would provide similar responses is high-pass enhancement of the transient of $c(t)$ and a larger value of $c_{\frac{1}{2}}$. This is a physiologically reasonable possibility, since it is known that the spatial pooling of the Y-cell non-linear network has high-pass characteristics (Victor & Shapley, 1979). Further definition of these dynamical details is likely to require appropriate intracellular studies.

Qualitative aspects of model behaviour

The proposed dynamical model has approximately linear behaviour near threshold, yet shows significant non-linearities in the moderate suprathreshold region (contrast 0·1 or greater). This non-linear behaviour causes an increased transience of responses to abrupt steps of contrast, yet does not introduce appreciable harmonic distortion into responses to sinusoidal stimulation.

Fig. 9 illustrates these phenomena. Responses to steps and sinusoids have been synthesized from a model with parameters set equal to the median of those observed for the on-centre X cell population. At low modulation depths, the linear model, the quasi-linear model, and the full dynamical model yield essentially indistinguishable results. At high modulation depths, the response to the step predicted by the linear model is not as 'transient' as the responses predicted by either the quasi-linear model or the full dynamical model.

As seen in Fig. 9, all three models predict essentially identical responses to sinusoids at low modulation depths. However, responses to sinusoids at high modulation depths are more attenuated at low temporal frequencies by the quasi-linear and dynamic non-linear models, as compared with the linear prediction. Most of the effect of the non-linearity is present in the quasi-linear model; the dynamic non-linear model introduces very slight additional attenuation and very little harmonic distortion. The harmonic distortion amounts to a third-harmonic/first-harmonic amplitude ratio of 5·7 % at 1·06 Hz, 2·2 % at 4·22 Hz and 0·1 % at 16·90 Hz. Thus, the effect of the dynamic non-linearity is likely to be hidden in experiments using sinusoidal stimuli. For these reasons, it is not surprising that linear models provide a reasonable picture of X cell responses in many circumstances (Rodieck, 1965; Maffei, Cervetto & Fiorentini, 1970; Hochstein & Shapley, 1976*a*, *b*; Enroth-Cugell, Robson, Schweitzer-Tong & Watson, 1983).

Third-harmonic responses are also not evident in response to sum-of-sinusoids input. This is because in an N-sinusoid experiment, the third-harmonic responses are spread over the $N(2N^2+1)/3$ third-order combination frequencies. The response to a step, however, reveals the effect of the non-linearity because the internal variable that adjusts dynamics, $c(t)$, has a sharp peak at the transient (Fig. 6). On the other hand, although the step responses show the presence of the non-linearity, they do not indicate which of the dynamical parameters is affected by contrast. This complementary information is provided by the sum-of-sinusoids responses.

X cell dynamics are those of an adaptive filter. When recent temporal fluctuations in the stimulus are small, the neural measure of contrast $c(t)$ is small, and the transfer characteristics pass low temporal frequencies relatively well. When recent temporal fluctuations in the stimulus are large, $c(t)$ is high, low frequencies are relatively suppressed, and tuning is shifted to higher frequencies. The contrast gain control is a deviation from linearity that allows the ganglion cell to shift its tuning to accommodate the temporal frequencies present in the input. This modulation is accomplished in such a way that harmonic distortion is minimal.

Physiological implications

Relationship to light adaptation. Viewed as an adaptive filter, the contrast gain control is closely analogous to the light adaptation processes that reside in the photoreceptors (Baylor & Hodgkin, 1974). At low light intensities, adaptation shifts the operating curve of the receptor left; at higher light intensities, it is shifted right. At any given light intensity, the receptor potential is approximately linear. The contrast gain control operates in a regime of relatively small luminance fluctuations, which does not significantly change the state of the luminance gain control. In both cases, the non-linear process may be viewed as a mechanism which adjusts the operating characteristics of the retina to allow better use of a finite range or band width. Both non-linear processes illustrate how a filter which adapts with a rapid time constant (Adelson, 1982) may be integrated into a system whose over-all behaviour is approximately linear.

Dispersion of dynamical parameters. As seen in Fig. 4 and Table 2, some of the model parameters (A, T_0 and $c_{\frac{1}{2}}$) vary strikingly across the population of retinal ganglion cells, while other parameters (N_L, T_L and H_S) are tightly clustered. (Because the analytical method cannot determine T_C precisely, its variability across the population cannot be assessed.) The variability of T_0 and $c_{\frac{1}{2}}$ implies substantially non-uniformity of the temporal tuning of receptive field centres, which will be further discussed below; the variability of A reflects variability of receptive-field centre sensitivity.

Some of the apparent variability in these parameters is due to the experimental procedure: the spatial frequency of the grating stimulus was chosen to be half of the grating resolution, so that surround responses would be neglible. However, in this spatial frequency range, the (spatial) modulation transfer function is very steep. Thus, a small change (20 %) in spatial frequency may result in a larger change (27 %) in the over-all size of the measured response, and similar change in the neural contrast signal.

Small errors in the choice of spatial frequency would have a similar effect on the estimate of $c_{\frac{1}{2}}$, since the effective contrast seen by receptive-field centres would be attenuated at higher spatial frequencies and enhanced at lower spatial frequencies. Thus, only a small portion of the more than tenfold variability of A and $c_{\frac{1}{2}}$ is explicable in terms of an error in the choice of spatial frequency. No effect of small errors in the estimate of spatial frequency resolution on the estimate of T_0 is anticipated, since T_0 is an extrapolation to a contrast of zero.

An additional source of variability in the estimated parameters may be animal-to-animal differences. However, there is comparable variability within preparations and across preparations. Thus, the observed variability reflects real physiological differences across the population of X cells. It is difficult to exclude completely long-term variations of responsivity consequent to deterioration of the physiological preparation with time. However, the general physiological status of the animal was closely monitored during the experiment, and data were collected only while the optics were satisfasctory. Furthermore, an over-all loss in responsivity would not explain changes in the dynamical parameters other than the absolute gain.

What does this variability suggest about retinal function? X cells show a marked variability in spatial scale both physiologically (Cleland, Levick & Sanderson, 1973;

Hochstein & Shapley, 1976*a*) and morphologically (Boycott & Wässle, 1974; Stone & Fukuda, 1974). However, the spatial variability is retinotopic: centre size is tightly linked to eccentricity (Cleland, Harding & Tulunay-Keesey, 1979). The variability of dynamics does not appear to be strongly retinotopic. Thus, at any retinal location, X cells have relatively similar spatial tuning but a wide range of dynamics. This has an interesting consequence for velocity tuning. Velocity tuning depends on both the spatial and temporal characteristics of the receptive field. Therefore, X cells at any retinal location will show a range of velocity tunings. The origin of this dispersion is the assortment of dynamic properties. Thus, the range of velocity tuning curves observed in central visual units (Movshon, Thompson & Tolhurst, 1978) may be derived from the range of dynamics present at the retinal level.

In many contexts there is a tradeoff of spatial and temporal resolution of the visual system (Wilson & Bergen, 1979). Well-known contributors to this phenomenon include the spatio-temporal coupling provided by centre–surround interactions (Enroth-Cugell *et al.* 1983) and the divergent properties of the X and Y cell systems (Lennie, 1980). The present results suggests that another source of the tradeoff is the variability of dynamics across the X cell population. Consider the retinal response to an abrupt stimulus change. In the early portion (< 100 ms) of the response, individual ganglion cell firing rates depend strongly on the high-pass parameters T_0 and $c_{\frac{1}{2}}$. Thus, the early response of a region of retina is rich in dynamical information encoded by ganglion cells with a range of temporal tuning. This dynamical information is at the sacrifice of positional information; fine positional information can only be extracted by comparing responses of nearby X cells with similar dynamics. However, once the typical T_0 is exceeded, responses depend only on A and H_S (and not on T_0, $c_{\frac{1}{2}}$, or T_C). Therefore, the late response dynamics are much more similar across the X cell population, since the values of H_S are tightly clustered. Late in the response, detailed dynamical information is sacrificed, but the full complement of X cells can be used to provide positional information.

Correlation with retinal anatomy. It is tempting to hypothesize a correspondence between the major components of the dynamical model and the morphology of the retina. Intracellular studies provide valuable clues to this end. We focus on the site of the high-pass stage, since this aspect of response dynamics is selectively modulated by the contrast gain control. Horizontal cell signals are well approximated by a low-pass transformation of the receptor response (van de Grind & Grusser, 1981); subtraction of such signals from the receptor potential provides a possible mechanism for generation of high-pass characteristics (Richter & Ullman, 1982). However, these experiments rule out any retinal mechanism with an effective summing area much larger than the receptive-field centre, because relatively high spatial frequencies are used. In particular, the spatial extent of an X cell surround is typically four times as large as the centre. If the surround provided a significant response at the test spatial frequency (an octave below the centre's resolution), then the total surround strength would have to be many times that of the centre, rather than approximately equal to that of the centre (Enroth-Cugell & Robson, 1966). Thus, it is unlikely that the horizontal cell is responsible for the high-pass component.

At the bipolar cell level, high-pass characteristics are evident in intracellular studies. In the photopic range, high-pass characteristics are evident in the light

response of photoreceptors themselves (Tranchina, Gordon, & Shapley, 1984; Daly & Normann, 1985). There is evidence for additional high-pass transformation the receptor-to-bipolar stage (Sakuranaga & Naka, 1985), and at the bipolar-to-ganglion cell stage (Toyoda, 1974). Our model, which contains only a single high-pass stage, provides a better fit to the observed transduction than a model with two or more high-pass stages (Shapley & Victor, 1981). However, this is only weak evidence against the presence of two or more high-pass stages – for some parameter ranges, the input–output properties of such models would not be readily distinguishable from a one-stage high-pass model.

The details of the contrast gain control are also relevant to hypotheses on the locus of the high-pass stage. Previously (Shapley & Victor, 1981), we suggested that the contrast gain control is a function of the inner plexiform layer. The neural measure of contrast is generated by a process of rectification. It has lateral spread, and is closely analogous to a non-linearity known to reside in the inner plexiform layer (Werblin & Copenhagen, 1974). The present analysis shows that the neural measure of contrast and the high-pass stage of the model are coupled by a non-linear interaction with a brief time constant T_C. This tight coupling suggests that at least a part of the high-pass transduction resides in the inner plexiform layer, where the neural measure of contrast is generated.

APPENDIX

The effect of a truncation non-linearity on apparent gain and mean firing rate

The transduction from a slow potential to an impulse train must be non-linear, because firing rates must be non-negative. This truncation is more likely to be manifest in units with a low maintained discharge or high gain than in units with a high maintained discharge or low gain. The truncation non-linearity causes the apparent gain A and mean firing rate M to deviate from the gain A_0 and mean rate M_0 that would be measured in the absence of truncation. Here we determine the size of these effects when the test signal is a sum-of-sinusoids stimulus presented at a modulation depth per sinusoid of m. The apparent gain $A(m)$ and mean firing rate $M(m)$ of a linear filter followed by this idealized spike generator are derived from analytic approximations for the zeroth- and first-order frequency kernels of this composite transduction.

Let the linear stage of the transduction be the filter G, with input $s(t)$ and output $y(t)$. Since G is linear, the Fourier transforms of the input $\tilde{s}(\omega)$ and the output $\tilde{y}(\omega)$ are related by the transfer function $\tilde{G}(\omega)$:

$$\tilde{y}(\omega) = \tilde{G}(\omega)\, \tilde{s}(\omega). \tag{9}$$

The output $y(t)$ of this linear stage is the input to a non-linear stage N. We postulate that the output of N, which is the instantaneous probability of a nerve impulse $r(t)$, is given by

$$r(t) = N(y(t)), \tag{10}$$

where

$$N(y) = \max\,(A_0 y + M_0,\, 0). \tag{11}$$

Here, M_0 is the mean firing rate in the absence of stimulation, and A_0 is the absolute gain, a proportionality constant between the output of the linear stage and the firing rate.

In general, the frequency kernels of a given non-linear system are closely approximated by the Wiener kernels of the system as measured with an appropriately matched Gaussian noise (Victor & Knight, 1979). It follows that the zeroth- and first-order frequency kernels at modulation depth m are closely approximated by

$$K_0(;m) \cong b_0, \tag{12}$$

and

$$\begin{aligned} K_1(f_j;m) &\cong 2 < b_1 y(t) . \exp[-i(2\pi f_j t + \phi_j)] > \\ &= b_1 m\tilde{G}(2\pi f_j). \end{aligned} \tag{13}$$

(The second step of eqn. (13) follows from eqn. (2) for $s(t)$ and eqn. (9)). The constants b_0 and b_1 are the first two coefficients in the Hermite expansion of the non-linearity N with respect to a Gaussian distribution of power (variance) P equal to the power passed by the linear filter G. The power P is proportional to the square of the modulation depth m:

$$P = \frac{1}{2}\sum_{j=1}^{8} m^2 . |\tilde{G}(2\pi f_j)|^2 = m^2 P_0. \tag{14}$$

The coefficients b_0 and b_1 are given by

$$b_0 = \int_{-\infty}^{\infty} N(y)\,\mathrm{Gau}(y,P)\,\mathrm{d}y, \tag{15}$$

and

$$b_1 = \frac{1}{P}\int_{-\infty}^{\infty} yN(y)\,\mathrm{Gau}(y,P)\,\mathrm{d}y, \tag{16}$$

where $\mathrm{Gau}(y,P)$ represents the Gaussian distribution of zero mean and variance P:

$$\mathrm{Gau}(y,P) = \frac{1}{(2\pi P)^{\frac{1}{2}}}\exp(-y^2/2P). \tag{17}$$

Note that because the power P depends on the modulation depth (eqn. (14)), so do the coefficients b_n and the frequency kernels K_n.

The coefficients b_0 and b_1 are calculated by substitution of the non-linearity function (11) into eqn. (15) and (16). It is convenient to use the dimensionless parameter

$$W(m) = M_0/(A_0 m \sqrt{P_0}), \tag{18}$$

which is the ratio of M_0 to the root-mean-squared depth of modulation seen by the non-linearity N. The results of these substitutions are:

$$K_0(;m) \cong M_0\left[\mathrm{erf}(W(m)) + \frac{1}{W(m)}\mathrm{Gau}(W(m),1)\right], \tag{19}$$

and

$$K_1(f_j;m) \cong m\tilde{G}(2\pi f_j)\, A_0\,\mathrm{erf}(W(m)). \tag{20}$$

The error function erf(W) is scaled so that erf($-\infty$) = 0, erf(0) = $\frac{1}{2}$ and erf($+\infty$) = 1:

$$\text{erf}(W) = \int_{-\infty}^{W} \text{Gau}(u, 1)\, du. \tag{21}$$

The mean firing rate $M(m)$ elicited by the sum-of-sinusoids signal at a modulation depth m is the zeroth-order frequency kernel (eqn. (19)). The frequency dependence of the first-order frequency kernel (eqn. (20)) is entirely due to the linear filter G, and is independent of modulation depth. (This independence would hold for any static non-linearity N, and not just the truncation non-linearity (11).) The apparent gain at the modulation depth m, $A(m)$, is the ratio of the first-order frequency kernel to the modulation depth m. Thus, $A(m)$ is given by

$$A(m) \cong A_0 \,\text{erf}(W(m)). \tag{22}$$

The model parameters A_0 and M_0 were determined by an iterative procedure to obtain the best match of eqns. (19) and (22) with the observed mean rates $M(m)$ and gains $A(m)$ at each modulation depth m.

Professors J. Gordon, E. Kaplan, B. Knight and R. Shapley contributed many helpful suggestions at all stages of this work. The numerous detailed comments of a reviewing Editor are gratefully appreciated. M. Conte, M. Greene, Y. Holland, C. Reid and R. Soodak provided excellent technical assistance. This work was supported in part by grants EY188, EY2439, EY6871 and NS877 from the United States National Institutes of Health, The Harry Frank Guggenheim Foundation, The Hardford Foundation and The McKnight Foundation.

REFERENCES

ADELSON, E. H. (1982). Saturation and adaptation in the rod system. *Vision Research* **22**, 1299–1312.

BAYLOR, D. A. & HODGKIN, A. L. (1974). Changes in time scale and sensitivity in turtle photoreceptors. *Journal of Physiology* **242**, 729–758.

BOYCOTT, B. B. & WÄSSLE, H. (1974). The morphological types of ganglion cells of the domestic cat's retina. *Journal of Physiology* **240**, 397–419.

BRODIE, S. E., KNIGHT, B. W. & RATLIFF, F. (1978). The response of the *Limulus* retina to moving stimuli: a prediction by Fourier synthesis. *Journal of General Physiology* **72**, 129–166.

CLELAND, B. G., DUBIN, M. W. & LEVICK, W. R. (1971). Sustained and transient neurones in the cat's retina and lateral geniculate nucleus. *Journal of Physiology* **217**, 473–496.

CLELAND, B. G., HARDING, T. H. & TULUNAY-KEESEY, U. (1979). Visual resolution and receptive field size: examination of two kinds of cat retinal ganglion cell. *Science* **205**, 1015–1017.

CLELAND, B. G., LEVICK, W. R. & SANDERSON, K. J. (1973). Properties of sustained and transient ganglion cells in the cat retina. *Journal of Physiology* **228**, 649–680.

DALY, S. J. & NORMANN, R. A. (1985). Temporal information processing in cones: effects of light adaptation on temporal summation and modulation. *Vision Research* **25**, 1197–1206.

EFRON, B. (1980). The jacknife, the bootstrap, and other resampling plans. Technical report no. 63, Division of Biostatistics, Stanford University, Stanford, CA., U.S.A.

ENROTH-CUGELL, C. & ROBSON, J. G. (1966). The contrast sensitivity of retinal ganglion cells of the cat. *Journal of Physiology* **187**, 517–552.

ENROTH-CUGELL, C., ROBSON, J. G., SCHWEITZER-TONG, D. E. & WATSON, A. B. (1983). Spatio-temporal interactions in cat retinal ganglion cells showing linear spatial summation. *Journal of Physiology* **341**, 279–307.

HOCHSTEIN, S. & SHAPLEY, R. M. (1976*a*). Quantitative analysis of retinal ganglion cell classifications. *Journal of Physiology* **262**, 237–264.

HOCHSTEIN, S. & SHAPLEY, R. M. (1976*b*). Linear and non-linear spatial subunits in Y cat retinal ganglion cells. *Journal of Physiology* **262**, 265–284.

KAPLAN, E. & SHAPLEY, R. M. (1984). The origin of the S (slow) potential in the mammalian lateral geniculate nucleus. *Experimental Brain Research* **55**, 111–116.

LENNIE, P. (1980). Parallel visual pathways: a review. *Vision Research* **20**, 561–594.

LEVICK, W. R. & THIBOS, L. N. (1982). Analysis of orientiation bias in cat retina. *Journal of Physiology* **329**, 243–261.

MAFFEI, L., CERVETTO, L. & FIORENTINI, A. (1970). Transfer characteristics of excitation and inhibition in cat retinal ganglion cells. *Journal of Neurophysiology* **33**, 276–284.

MILKMAN, N., SCHICK, G., ROSSETTO, M., RATLIFF, F., SHAPLEY, R. & VICTOR, J. (1980). A two-dimensional computer-controlled visual stimulator. *Behavioural Research Methods and Instrumentation* **12**, 283–292.

MOVSHON, J. A., THOMPSON, I. D. & TOLHURST, D. J. (1978). Spatial and temporal contrast sensitivity of neurones in areas 17 and 18 of the cat's visual cortex. *Journal of Physiology* **283**, 101–120.

RICHTER, J. & ULLMAN, S. (1982). A model for the temporal organization of X- and Y-type receptive fields in the primate retina. *Biological Cybernetics* **43**, 127–145.

RODIECK, R. W. (1965). Quantitative analysis of cat retinal ganglion cell response to visual stimuli. *Vision Research* **5**, 583–601.

RODIECK, R. W., PETTIGREW, J. D., BISHOP, P. O. & NIKARA, T. (1967). Residual eye movements in receptive-field studies of paralyzed cats. *Vision Research* **7**, 107–110.

SAKURANAGA, M. & NAKA, K.-I. (1985). Signal transmission in the catfish retina. I. Transmission in the outer retina. *Journal of Neurophysiology* **53**, 373–389.

SHAPLEY, R. M. & VICTOR, J. D. (1978). The effect of contrast on the transfer properties of cat retinal ganglion cells. *Journal of Physiology* **285**, 275–298.

SHAPLEY, R. M. & VICTOR, J. D. (1979). Non-linear spatial summation and the contrast gain control of cat retinal ganglion cells. *Journal of Physiology* **290**, 141–161.

SHAPLEY, R. M. & VICTOR, J. D. (1980). The effect of contrast on the non-linear response of the Y cell. *Journal of Physiology* **302**, 535–547.

SHAPLEY, R. M. & VICTOR, J. D. (1981). How the contrast gain control modifies the frequency response of cat retinal ganglion cells. *Journal of Physiology* **318**, 161–179.

SHAPLEY, R. & VICTOR, J. D. (1986). Hyperacuity in cat retinal ganglion cells. *Science* **231**, 999–1002.

STONE, J. & FUKUDA, Y. (1974). Properties of cat retinal ganglion cells: a comparison of W cells with X and Y cells. *Journal of Neurophysiology* **37**, 722–748.

TOYODA, J.-I. (1974). Frequency characteristics of retinal neurons in the carp. *Journal of General Physiology* **63**, 214–234.

TRANCHINA, D., GORDON, J. & SHAPLEY, R. M. (1984). Retinal light adaptation – evidence for a feedback mechanism. *Nature* **310**, 314–316.

VAN DE GRIND, W. & GRUSSER, O.-J. (1981). Frequency transfer properties of cat retina horizontal cells. *Visual Research* **21**, 1565–1572.

VICTOR, J. D. (1985). The non-linear dynamics of the center mechanism of cat retinal ganglion cells. *Proceedings of the IEEE International Conference on Systems, Man, and Cybernetics, Tucson, Arizona*, 867–873.

VICTOR, J. D. & KNIGHT, B. W. (1979). Non-linear analysis with an arbitrary stimulus ensemble. *Quarterly of Applied Mathematics* **37**, 113–136.

VICTOR, J. D. & SHAPLEY, R. M. (1979). The non-linear pathway of Y ganglion cells in the cat retina. *Journal of General Physiology* **74**, 671–689.

VICTOR, J. D. & SHAPLEY, R. M. (1980). A method of non-linear analysis in the frequency domain. *Biophysical Journal* **29**, 459–484.

WERBLIN, F. S. & COPENHAGEN, D. R. (1974). Control of retinal sensitivity. III. Lateral interactions at the inner plexiform layer. *Journal of General Physiology* **63**, 88–110.

WILSON, H. R. & BERGEN, J. R. (1979). A four mechanism model for threshold spatial vision. *Vision Research* **19**, 19–32.